University of Groningen

The mechanical response of lithographically defined break junctions

Huisman, E. H.; Trouwborst, M. L.; Bakker, F. L.; van Wees, Bart; van der Molen, S. J.

IMPORTANT NOTE: You are advised to consult the publisher's version (publisher's PDF) if you wish to cite from it. Please check the document version below.

Document Version
Publisher's PDF, also known as Version of record

Publication date:
2011

[Link to publication in University of Groningen/UMCG research database](#)

The mechanical response of lithographically defined break junctions

E. H. Huisman,[1,a)] M. L. Trouwborst,[1,2] F. L. Bakker,[1] B. J. van Wees,[1]
and S. J. van der Molen[2]

[1]*Physics of Nanodevices, Zernike Institute for Advanced Materials, University of Groningen, Nijenborgh 4, 9747 AG Groningen, The Netherlands*
[2]*Kamerlingh Onnes Laboratory, Leiden University, P.O. Box 9504, 2300 RA, Leiden, The Netherlands*

We present an experimental study on the mechanical response of lithographically defined break junctions by measuring atomic chain formation, tunneling traces and Gundlach oscillations. The calibration factor, i.e., the ratio between the electrode movement and the bending of the substrate, is found to be 2.5 times larger than expected from a simple mechanical model. This result is consistent with previous finite-element calculations. Comparing different samples, the mechanical response is found to be similar for electrode separations >4 Å. However, for smaller electrode separations significant sample-to-sample variations appear. These variations are ascribed to differences in the shape of the two electrodes on the atomic scale which cannot be controlled by the fabrication process. © *2011 American Institute of Physics*. [doi:10.1063/1.3587192]

I. INTRODUCTION

A surprisingly simple way to create stable atomic point contacts is provided by the mechanically controllable break junction (MCBJ) technique. MCBJs are very insensitive to mechanical vibrations, show negligible drift and can be stretched with an impressive resolution ($\approx$ picometers).[1–3] These characteristics make MCBJs very suitable for investigating charge transport through single or a small number of atoms or molecules.[4–13] Moreover, electron beam lithography makes it possible to fabricate these junctions in a fully reproducible way. However, systematic experimental studies on the mechanical response of lithographically defined junctions are scarce.[14,16] This is surprising since knowledge of the mechanical response is often crucial for the interpretation of experimental results.[5,12] Previously, Vrouwe *et al*. have calculated the mechanical response of lithographically defined MCBJs using a finite element analysis.[14] They predict that the response is strongly affected by the softness of the underlying polyimide layer. In this paper, we investigate the mechanical properties of lithographically defined MCBJs in detail, using three different techniques; atomic chain formation, tunneling traces and Gundlach oscillations.

Let us start by discussing the basic principle of the break junction technique. The lower panel of Fig. 1 shows a schematic drawing of a lithographically defined break junction. Basically, it consists of a gold strip patterned on top of a flexible substrate. A polyimide film is used to electrically isolate the gold strip from the substrate. By bending the substrate the strip stretches in the lateral direction, thins down and finally breaks at the center. The strength of the break junction technique immediately follows from the ratio of the stretching of the wire Δd and the bending of the substrate ΔZ. This is often called the attenuation factor or calibration factor r, given by:[3,14]

$$r = \frac{\Delta d}{\Delta Z} = \zeta \frac{6tU}{L^2} \qquad (1)$$

Here, t is the thickness of the substrate, U is the suspended bridge length and L is the distance between the counter supports. ζ is a correction factor which is added to account for the elastic properties of the polyimide layer.[14] To accurately determine ζ is a central goal of this study. For our junctions, L = 18.8 $\pm$0.1 mm, t = 0.42 $\pm$0.05 mm and U = 2.4 $\pm$0.3 μm, resulting in an uncorrected attenuation ($\zeta = 1$) of r = 1.7 $\pm$0.2 10^{-5}. Multiplying this factor with the bending resolution ($\Delta Z = 0.1$ μm) gives an impressive resolution ($\sim 10^{-12}$m). This attenuation factor and the very small mechanical loop (<3 μm) make lithographically defined break junctions highly stable. As a practical consequence, atomic point contacts can be studied without the need of a vibration isolation system around the measurement setup. In contrast, vibration isolation is crucial for creating atomic contacts using a scanning tunneling microscope (STM) or nonlithographic break junctions with their larger mechanical loops.[17,19,21]

For typical break junction geometries Vrouwe *et al*. predicted ζ to be between two and four.[14] This correction is related to the elasticity of the polyimide layer which effectively increases U. Here, we present a combined experimental study to determine the attenuation factor of lithographically defined break junctions. We use three different calibration techniques in three different inter-electrode regimes. Figure 1 shows these regimes in more detail: atomic chain formation (regime I, d < 0), direct vacuum tunneling (regime II, 0 < d < 0.5 nm) and Gundlach oscillations (regime III, d > 1 nm). Each regime is explained below.

Our experimental results are consistent with the value anticipated by Vrouwe *et al*. ($\zeta \approx 3$ for our geometry[15]). However, sample-to-sample variations are observed in the

---
a)Present address: Center for Electron Transport in Molecular Nanostructures, Columbia University, 500 West 120th St., New York, NY 10027, USA. Electronic mail: ehh2125@columbia.edu.
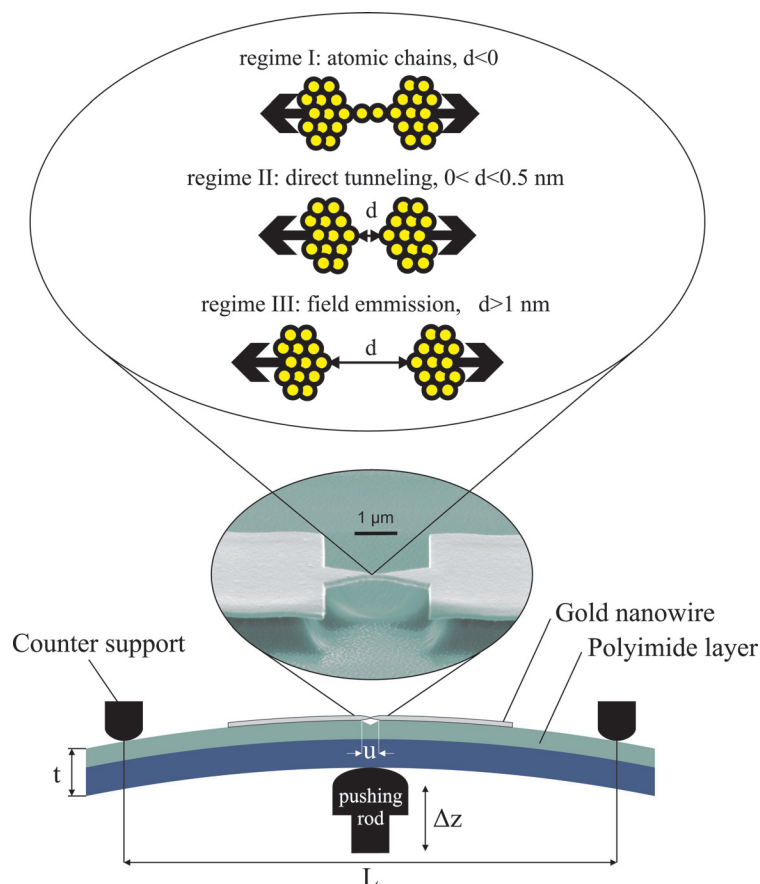
FIG. 1. (Color online) Bottom panel: schematic drawing of a lithographically defined break junction. By bending the substrate the wire is thinned down until it eventually breaks. Then, the electrode spacing d can be precisely controlled. Middle panel: Scanning electron micrograph of a break junction showing the under etched gold bridge on top of the polyimide layer. Top panel: representation of the three distance regimes studied. Regime I ($d < 0$ nm): Formation of atomic chains just before the wire breaks. Regime II ($0 < d < 0.5$ nm): Direct vacuum tunneling. Regime III ($1 < d < 10$ nm): Field emission or Fowler Nordheim tunneling.

mechanical response for small electrode separations (<4 Å). These are explained by variations in the shape of the electrodes.

II. EXPERIMENTAL SETUP

To fabricate lithographically defined MCBJs we used the same design as used by Vrouwe *et al.*[14] A polyimide layer is spincoated (thickness three μm) on top of a polished phosphor bronze substrate (thickness 0.42 mm) to electrically isolate the substrate. Subsequently, a gold strip is patterned on top of the polyimide layer with electron beam lithography (EBL) and metal evaporation (thickness 120 nm). Finally, the polyimide layer is etched to create a free hanging gold bridge (see inset in Fig. 1). For a detailed description, we refer to Refs. 3 and 14. For an experiment, a break junction is mounted in a three-point bending bench within a low-temperature insert. All experiments are performed in cryogenic vacuum at T $\approx$ 5 K to exclude the influence of adsorbates and to reduce the thermal motion of the atoms. The conductance is measured by applying a constant voltage of typically 100 mV while measuring the current.

III. RESULTS

A. Chain formation

The first calibration technique which we discuss is atomic chain formation. Figure 2 shows a typical plot of the conductance of a break junction as a function of the position of the pushing rod. By bending the substrate with the pushing rod, the wire is extended and will eventually break at the constriction. Clearly, the conductance of the junction decreases stepwise while stretching. This is related to the stepwise decrease of the number of atoms in the constriction. Just before breaking, a long conductance plateau is observed around 1 G_0, which corresponds to a contact with a diameter of a single atom.[2] However, the length of this plateau is often much longer than the length of a single atom. This can be understood by realizing that for a number of metals including gold, the binding energy of an atom in a chain is larger than the binding energy of an atom in bulk metal.[2,18] As a consequence, just before the wire breaks, atoms are pulled out of the electrodes and tend to form chains up to a few atoms in length. This intriguing phenomenon was studied by Yanson *et al.*,[17] who measured the length of conductance plateaus around one G_0. By plotting the distribution of plateau lengths of a large number of breaking traces, peaks are observed in the histogram (see inset in Fig. 2). Since the plateaus consist of an integer number of atoms, the spacing between the peaks (in units of pushing rod displacement) is equal to the size of an atom. Hence, plateau length histograms can be used as a calibration method.

For the junction characterized in Fig. 2, the distance between the first two peaks is 4.9 ± 0.8 μm, which corresponds to the gold-gold bond length of 2.5 $\pm$ 0.2 Å[19] in a chain. This gives us the attenuation factor of this junction of r $= (5.1 \pm 1) \times 10^{-5}$. Taking the uncorrected attenuation for our junctions of 1.7×10^{-5} (as calculated in the introduction), we find a correction factor of $\zeta = 3.0 \pm 0.6$. This value is in agreement with the prediction by Vrouwe *et al.*
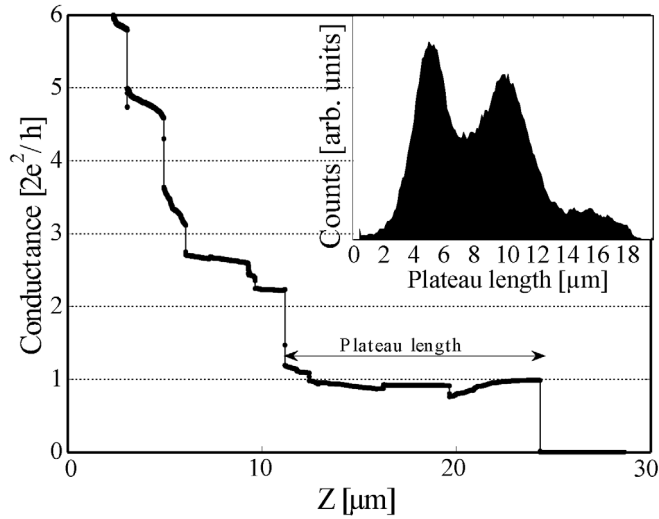
FIG. 2. Conductance of a gold junction while stretching. Just before breaking, the conductance shows a long plateau around one G_0 which is attributed to the formation of an atomic chain. The plateau length is defined as the length where the conductance is in between $1.2 G_0 > 0.7 G_0$. Inset: Histogram of the plateau lengths of 1100 pulling traces. In between each trace, the junction was closed up to 20 G_0. The bin size is 0.11 μm and the histogram is averaged over 15 bins (V_{bias} = 100 mV).

We note that this is the first time that a 1 G_0 plateau length histogram is constructed for a lithographically defined MCBJ. In our case, the pushing rod is moved with a speed of one μm/s. Using the calibration factor calculated above, this corresponds to an electrode speed of only 0.05 nm/s. This is much slower than the effective speeds used in notched wire break junctions[17] or STM (Ref. [19]) ($\approx$10 nm/s). Nevertheless, two well-defined peaks appear in the histogram and the onset of a third peak is visible. This shows that chains with two or even three atoms occur frequently in lithographically defined MCBJs and indicates that the formation of atomic chains is not limited by mechanical vibrations. Finally, we note that the intensity of the peaks in the histogram may vary for different samples. In about 20 % of the samples, no structure is observed at all. This is probably related to the shape of the electrodes and will be further discussed in Sec. IV.

B. Gundlach oscillations

The second calibration technique used is Gundlach oscillations.[19–21] Gundlach oscillations appear in the tunneling conductance when a bias voltage V_{bias} is applied which exceeds the work function of the electrodes. This regime is called field-emission or fowler-nordheim (FN) tunneling and is explained in Fig. 3. In the FN regime, part of the barrier becomes classically available. As a consequence, the electrons will partly reflect on both edges of a triangular well, such that a standing wave pattern develops for each electron wave harmonic n. These harmonics can be observed in the differential conductance. For each n, the differential conductance will peak at a bias voltage $V_n = \varphi/e + (3\pi\hbar/2e\sqrt{2m})^{2/3}F^{2/3}n^{2/3}$(Ref. [21]). Here, F is the electric field strength. As we will see below, V_n and n can be determined

from experiment, such that F, the work function φ and eventually the attenuation factor can be derived.

The idea of the experiment is to measure the differential conductance (dI/dV) at fixed electric field while varying the distance d. This way, the width of the classically available region is being increased while the shape of the triangular barrier remains the same. Experimentally, this is realized as follows. First, the wire is broken and opened to an inter-electrode distance of approximately one nm. Then, a DC bias voltage is applied such that a setpoint current of one nA is reached. Subsequently, the differential conductance is measured using a lock-in technique with an AC voltage of 100 mV on top of the DC bias voltage. Finally, the motor position Z is increased with a fixed step of 0.05 μm and the whole procedure is repeated until a bias voltage of typically 16 V is reached. A resulting Gundlach measurement is plotted in Fig. 4(a). As expected, a clear oscillating pattern is observed with the first maximum in the differential conductance just above the work function of gold (around 5.4 eV). In Fig. 4(b), the position of the maxima are plotted as a function of the peak index. From the linear relation for higher peak index, an electric field strength is obtained of 2 V/nm. The electric field strength, together with the relation between the motor position and bias voltage plotted in Fig. 4(a), yields the attenuation factor of the junction.

For this junction, we find r = $(4.2 \pm 0.5) \times 10^{-5}$. Again, using the uncorrected attenuation of 1.7×10^{-5} we find a correction factor of $\zeta = 2.5 \pm 0.3$. This value is close to the factor found using plateau length histograms ($\zeta = 3.0 \pm 0.6$). We have repeated the Gundlach measurements on four different samples, see Table I. Interestingly, similar ζ values were obtained for different samples which shows that the break junctions are fabricated in a reproducible way.

Finally, as discussed above, Gundlach oscillations can also be used to deduce the work function of the electrodes [see Fig. 4(b)]. Values were obtained between 4.9 eV and
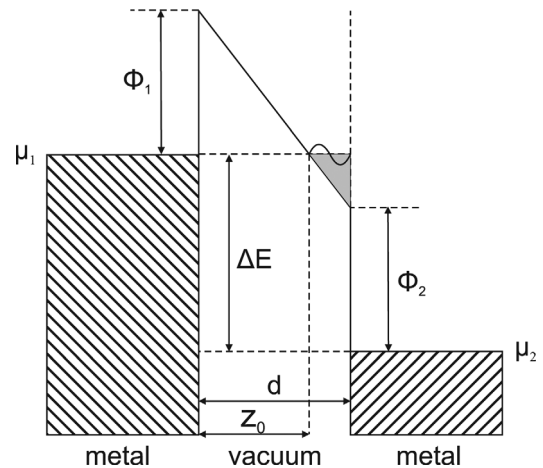

FIG. 3. Energy band diagram for the Fowler-Nordheim regime. For bias voltages higher than the work function of the metal, $V > \varphi/e$, part of the barrier becomes classically available. This gives rise to a new interface, as denoted by Z_0. In between this interface and the right electrode, a part arises where the electron wave functions interfere (gray). This interference pattern influences the total transmission coefficient and is sensitive to the bias voltage and the electrode separation.
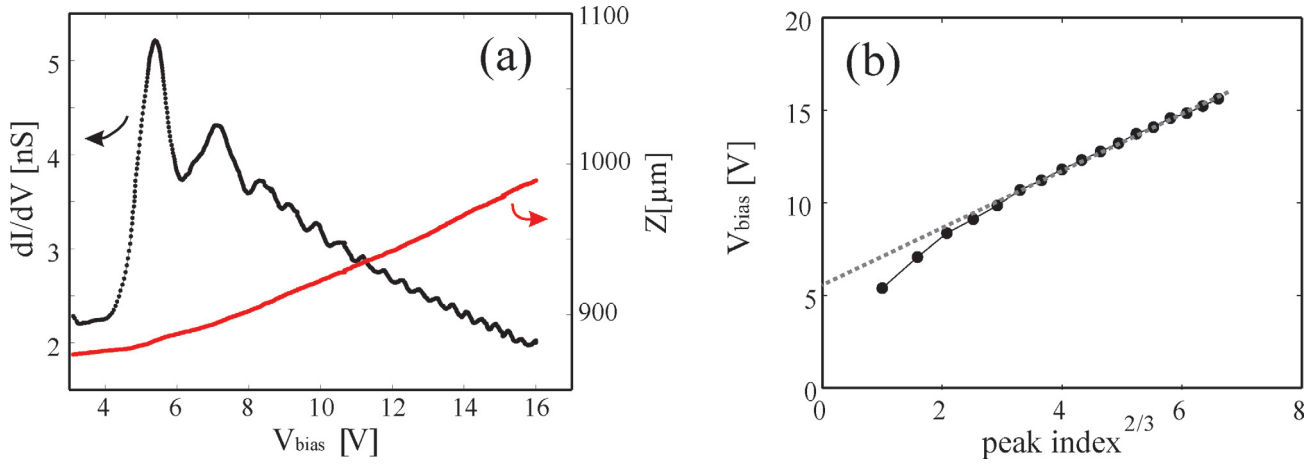
FIG. 4. (Color online) (a) Black dotted curve: differential conductance as a function of the bias voltage for sample A. For each value of the bias voltage, the pushing rod position is adjusted such that the current is 1 nA (red solid line). Above 8 V, there is a linear relation between motor position and bias voltage. The differential conductance is measured using a standard Lock-in technique (AC signal is 100 mV) (b) Plot of the peak index vs the position of the maxima at the voltage axis. For higher peak index, the relation is linear and the work function can be extracted from the interception with the voltage axis (here 5.6 eV).

5.6 eV, as given in Table II. Within their error, these values agree with the literature values for the work function of gold (5.3 to 5.5 eV, dependent on surface structure)[22] which shows that the surface of the electrodes is free of adsorbates. Also, we have checked the reproducibility of the measurements by repeating the Gundlach experiments on sample D. In between the measurements, the junction was closed to a conductance of 5 G_0 to randomize the shape of both electrodes.[7] We find equal values for ζ of 2.4 ± 0.2 for both runs, and the two work functions for both contacts are similar (first run: $\varphi = 5.2 \pm 0.2$ eV, second run $\varphi = 4.9 \pm 0.3$ eV).

C. Tunneling current

The third calibration method which is discussed is formed by tunnel current measurements as a function of inter electrode distance. For bias voltages much smaller than the work function of the electrodes, the tunnel current can be approximated by $G(d) \propto \exp[(-d/\hbar)\sqrt{8m\varphi}]$ (Refs. 23 and 24). Here, φ is the work function of the metal and m is the electron mass. Hence, when plotting the logarithm of the current as a function of distance one obtains a straight line with slope $(\Delta^{10}\log G/\Delta d) = (-\sqrt{8m\varphi}/\hbar \times \ln 10)$. Taking 5.4 eV for the work function of gold, this relation can be used to calibrate the junction.

TABLE I. Correction factors (ζ) for the attenuation of break junctions, measured on five different samples with three different calibration techniques. Each letter corresponds to a different sample. For sample *D* we have performed two independent Gundlach experiments by closing the junction in between the measurements. Regarding the tunnel slope measurements, the slope is measured in between 2×10^{-5} and 2×10^{-4} G_0.

Sample	Plateau length	Tunnel slope	Gundlach oscillations
A	-	-	2.5±0.3
B	-	2.6±0.7	2.6±0.3
C	-	2.3±0.6	1.9±0.2
D (1)	-	2.4±0.7	2.4±0.2
D (2)	-	2.4±0.7	2.4±0.2
E	3.0±0.6	2.3±0.5	-

In Fig. 5(a), five typical closing traces are shown of the tunnel current versus the pushing rod position. In between each trace, the junction is closed to a conductance value of >20 G_0 which leads to a reorganization of the contact. As described above, the tunnel current is expected to decay exponentially with distance. Still, variations in exponential decay are observed. To map these variations, we determined the tunnel slopes of 1100 traces at relatively large distance (between $2 \times 10^{-5}G_0 < G < 2 \times 10^{-4}G_0$). This is shown in Fig. 5(c). We find an average slope of -0.4 ± 0.1 μm^{-1}, resulting in an attenuation of r $= (3.9 \pm 0.9) \times 10^{-5}$. This corresponds to a correction factor of $\zeta = 2.3 \pm 0.5$. In total, we calibrated 4 samples using this slope method, all resulting in similar values for ζ, see Table I.

The spread in Fig. 5(c) indicates that there is a large difference in tunnel slope each time a new contact is formed. In fact, similar variations have been reported on notched wire break junctions and scanning tunneling microscopes.[25,26] Partly, this variation can be explained by the three-dimensional nature of the electrodes and variations in the work function. For example, it is well known that the work function is dependent on the crystal orientation of the electrodes (e.g., the work function for gold (100) is 5.47 eV while for gold(111) it has a value of 5.31 eV) (Ref. 22). Indeed, each time a new contact is formed the atoms forming the apex of the electrodes will be modified. This is expected to give a variation in the work function. A second explanation of the spread in Fig. 5(c) may be formed by imperfections in the mechanical

TABLE II. Work functions for five different samples as obtained from the Gundlach measurements. Each letter corresponds to a different sample.

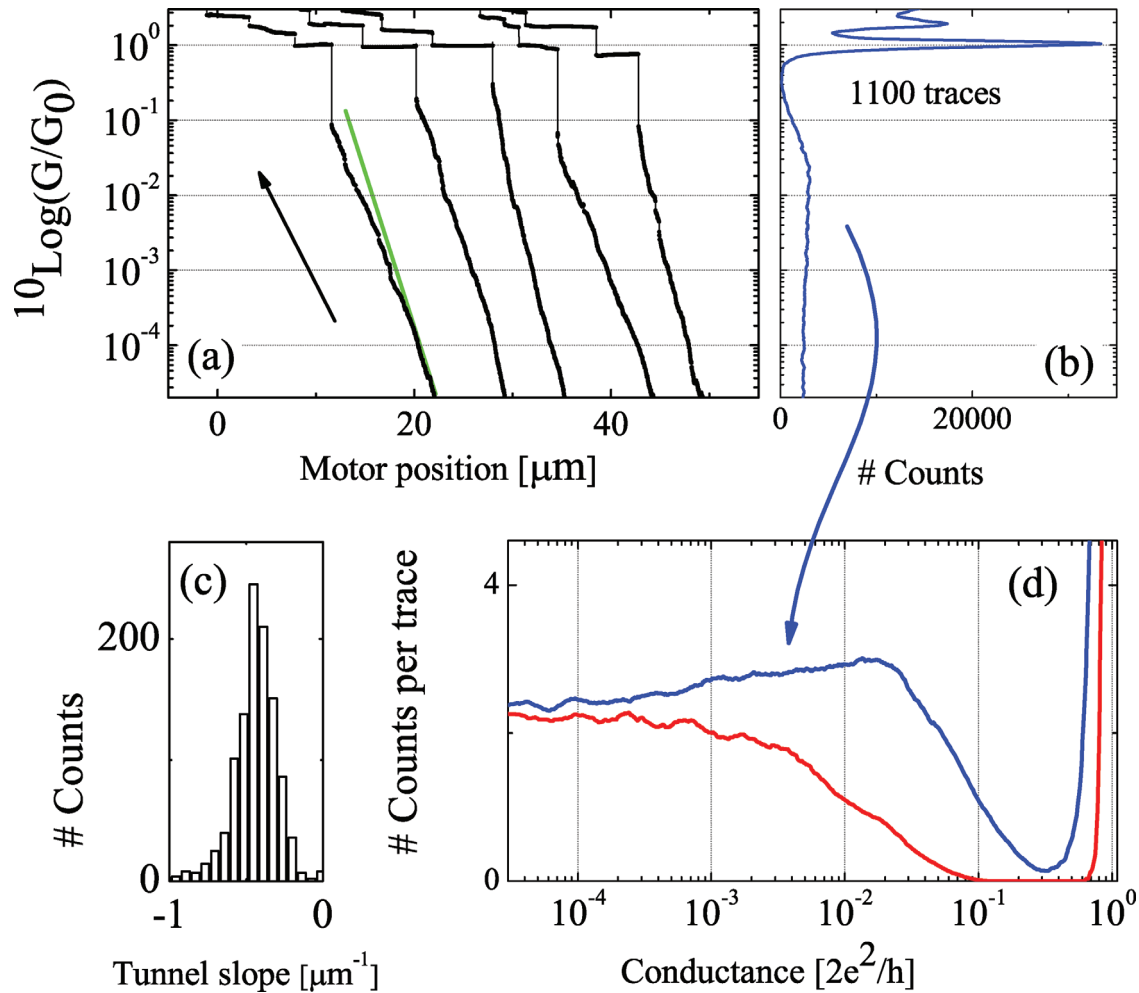| Sample	Work function [eV]
A	5.6±0.2
B	5.1±0.2
C	5.5±0.3
D (1)	5.2±0.2
D (2)	4.9±0.3

FIG. 5. (Color online) (a) Five typical closing traces of sample E showing the tunnel current as a function of pushing rod position. (b) Histogram of 1100 closing traces of sample E. In between each trace, the junction is closed up to 20 G_0. (c) Histogram of slopes in the tunnel regime obtained from 1100 closing traces (sample E). The slope was determined by fitting the data in the conductance range between 2×10^{-5} and 2×10^{-4} G_0. (d) Histogram of closing traces for sample E (blue, upper curve) and sample C (red, lower curve). For conductance values $<10^{-4}G_0$, the number of counts is similar for both junctions. In contrast, the number of count varies significantly for conductance values $>10^{-4}G_0$.

transmission between the motor and the substrate. However, this will not affect the average value for the tunnel slope.

Remarkably, deviations from exponential decay were observed for small electrode separations. Furthermore, despite the fact that different samples give a similar average ζ for $G < 2 \times 10^{-4}G_0$, we found significant sample-to-sample variations when the calibration factor was determined at smaller electrode separations. To illustrate this, we plotted conductance histograms of the closing traces for two different samples [see Fig. 5(d)]. In this representation, a constant tunnel slope would give a horizontal line in the conductance histogram.[12] Indeed, the histograms of the two samples have approximately the same number of counts for $G < 2 \times 10^{-4}G_0$. Thus, the two samples have the same calibration factor. However, a large difference in counts can be observed for the higher conductance regime. This observation will be further discussed below.

IV. Sample-to-sample variations

To explain the large variation in counts per conductance value for the two samples plotted in Fig. 5(d), it is needed to

understand the different contributions to such a histogram. First of all, both histograms show — although at a somewhat different conductance — a strong decrease in counts just before closing. This is due to the so-called Jump to Contact[7,27] at small electrode distances when atomic binding forces cause the last atoms of each electrode to fuse. This is clearly shown in the traces plotted in Fig. 5(a), where the conductance suddenly jumps to 1 G_0, forming a single atom contact. To further examine the influence of the Jump to Contact on the histogram shape, we determined the conductance value G_{JC} of each trace right before it jumps. Figure 6(a) shows the resulting distributions for both samples shown in Fig. 5(b). The spread in the G_{JC} distribution explains why a gradual (rather than an abrupt) decrease is observed in counts above $10^{-2}G_0$ in the histograms of Fig. 5(b). Furthermore, the average G_{JC} for sample E is substantially higher than for sample C, indicating sample E has on average 'stiffer' electrodes.[7]

Taking into account the decrease in counts due to the Jump to Contact, the histogram will have a shape like curve two in Fig. 6(d), provided the electrodes approach head-on [cf. sample C in Fig. 5(d)]. Without the Jump to Contact, the curve would be a horizontal line like curve one. Clearly, this
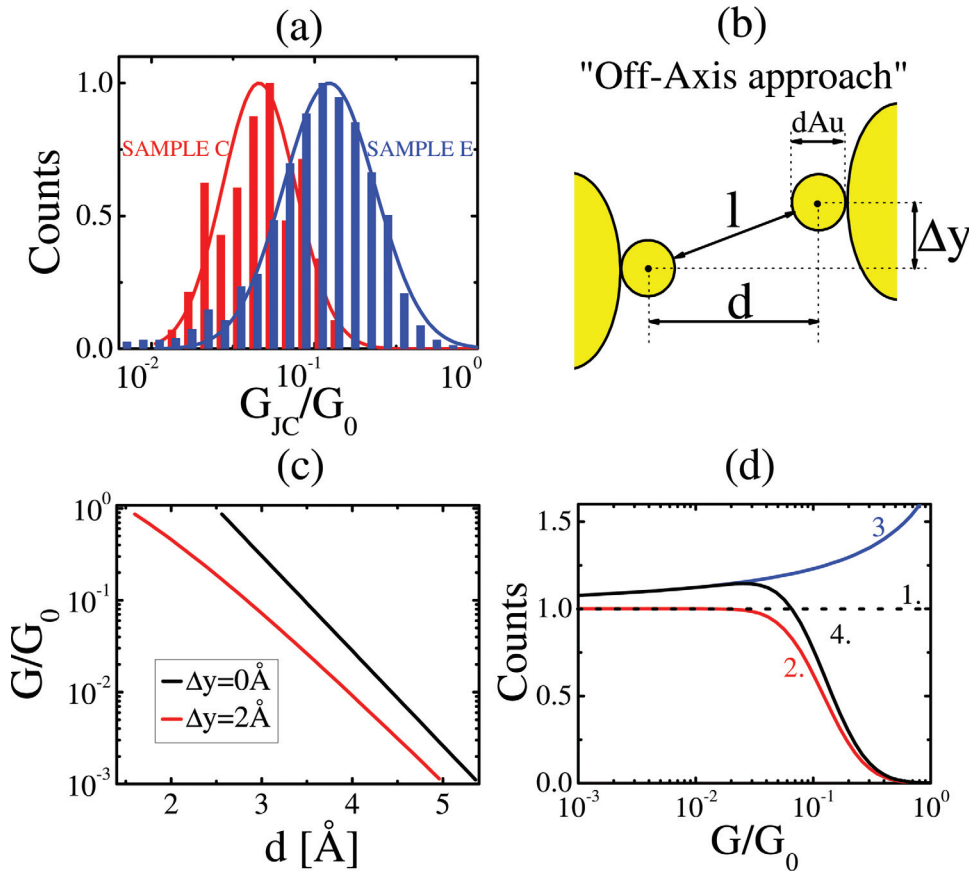
FIG. 6. (Color online) (a) Measured distribution of the conductance value just before Jump to Contact G_{JC} for both samples plotted in Fig. 5(d). (b) Model for the 'off-axis approach.' The effective tunneling distance l is given by $\sqrt{d^2 + \Delta y^2} - d_{Au}$ (d_{Au} is the diameter of a gold atom, 2.5 Å[19]). (c) If there were no Jump to Contact and the last apex atoms are perfectly aligned with the central axis of deflection, $\Delta y = 0$, the tunnel slope is constant and does not depend on distance. In contrast, a small offset from this axis, say $\Delta y = 2$ Å, results in a reduced tunnel slope for small d. (d) Model for the shape of the histogram. (1) Histogram when assuming a constant barrier height up to closing and no Jump to Contact (dashed black line). (2) Histogram taking into account the Jump to Contact distribution of sample E plotted in panel (a) (red line). The number of counts decreases for conductance values $>10^{-2}G_0$. (3) Histogram when assuming an off-axis approach ($\Delta y = 2$ Å) plotted in panel (b) (blue line). (4) Final curve taking into account both the Jump to Contact and the 'off-axis approach' (solid black line). The shape of this histogram is qualitatively in agreement with the observed histogram for sample E in Fig. 5.

does not explain all differences between the two samples. In fact, the number of counts of sample *E* even *increases* before decreasing, indicating the slope decreases just before jumping to contact. We propose that the reduced slope observed for smaller distances can be caused by a small offset Δy between the last apex atoms with respect to the central axis of deflection.[25] This so-called 'off-axis approach' is depicted in Fig. 6(b). When closing, the effective tunnel distance is now approximately given by $l = \sqrt{d^2 + \Delta y^2} - d_{Au}$, where Δy is the offset and d_{Au} the diameter of a gold atom. Figure 6(c) shows the effect of an offset when the conductance is plotted as a function of electrode separation d. For a junction without an offset (black line, $\Delta y = 0$), the conductance increases exponentially with distance. However, a small offset between the last apex atoms causes a decreased tunnel slope when approaching (red line, $\Delta y = 2$Å). When constructing a histogram for such a junction, an increase in counts is observed. Curve three in Fig. 6(d) gives the histogram constructed virtually out of traces with $\Delta y = 2$ Å. Also including the JC-distribution, we obtain curve four in Fig. 6(d). Interestingly, this histogram qualitatively matches the observed histogram for sample *E*. Hence, we propose that the last apex atoms on each electrode of sample *E* are slightly offset from the central axis of deflection. This is very well possible since it is well known that a metal wire often breaks along a grain boundary. Depending on the orientation of the grain boundaries, contacts with different off-axis offsets can be formed.[28] It is important to note that the orientation of the grain boundaries cannot be controlled by our

current fabrication process. Hence, sample-to-sample variations in the mechanical response of the break junctions will always appear for small electrode separations.

V. CONCLUSION

We have investigated the mechanical response of lithographically defined break junctions by measuring atomic chain formation, Gundlach oscillations and tunneling curves on five different samples in cryogenic vacuum. The different calibration techniques yield the same correction value $\zeta \approx 2.5$, within the experimental error. This value is consistent with the calculations of Vrouwe *et al.*, emphasizing the importance of the soft polyimide layer on which the junction rests. Interestingly, for small electrode separations (<4Å), sample-to-sample variations are observed both in the Jump to Contact and the tunnel slope. We provide evidence that these differences originate from variations in the junction's atomic structure. These cannot be controlled by lithography, but are of importance if small molecules are studied.

ACKNOWLEDGMENTS

[1]J. Moreland and J.W. Ekin, J. Appl. Phys. **58**, 3888 (1985); J. Moreland and P. K. Hansma, Rev. Sci. Instrum. **55**, 399 (1984).

[2]N. Agraït, A. L. Yeyati, and J. M. van Ruitenbeek, Phys. Rep. **377**, 81 (2003).

[3]J. M. van Ruitenbeek, A. Alvarez, I. Piñeyro, C. Grahmann, P. Joyez, M. H. Devoret, D. Esteve, and C. Urbina, Rev. Sci. Instrum. **67**, 108 (1996).

[4]C. Kergueris, J. P. Bourgoin, S. Palacin, D. Esteve, C. Urbina, M. Magoga, and C. Joachim, Phys. Rev. B **59**, 012505 (1999).

[5]J. Reichert, R. Ochs, D. Beckmann, H. Weber, M. Mayor, and H. v. Lohneysen, Phys. Rev. Lett. **88**, 176804 (2002).

[6]R. H. M. Smit, Y. Noat, C. Untiedt, N. D. Lang, M. C. van Hemert, and J. M. van Ruitenbeek, Nature **419**, 906 (2002).

[7]M. L. Trouwborst, E. H. Huisman, F. L. Bakker, S. J. van der Molen, and B. J. van Wees, Phys. Rev. Lett. **100**, 175502 (2008).

[8]C. A. Martin, D. Ding, H. S. J. van der Zant, and J. M. van Ruitenbeek, New J. Phys **10**, 065008 (2008).

[9]M. L. Trouwborst, E. H. Huisman, S. J. van der Molen, and B. J. van Wees, Phys. Rev. B **80**, 081407 (2009).

[10]E. Lörtscher, H. B. Weber, and H. Riel, Phys. Rev. Lett. **98**, 176807 (2007).

[11]E. H. Huisman, M. L. Trouwborst, F. L. Bakker, B. de Boer, B. J. van Wees, and S. J. van der Molen, Nano Lett. **8**, 3381 (2008).

[12]M.T. Gonzàlez, S. Wu, R. Huber, S.J. van der Molen, C. Schönenberger, and M. Calame, Nano Lett. **6**, 2238 (2006).

[13]D. den Boer, M. J. J. Coenen, M. van der Maas, T. P. J. Peters, O. I. Shklyarevskii, J. A. A. W. Elemans, A. W. Rowan, and S. Speller, J. Phys. Chem. C **113**, 15412 (2009).

[14]S. A. G. Vrouwe, E. van der Giessen, S. J. van der Molen, D. Dulic, M. L. Trouwborst, and B. J. van Wees, Phys. Rev. B. **71**, 035313 (2005).

[15]The value predicted for our geometry equals $\zeta = 2$. However, the presence of the leads, which are not included in the calculations of Vrouwe *et al.*, will result in a somewhat higher $\zeta \approx 3$.

[16]L. Grüter, "Mechanical Controllable Break Junction in Liquid Environment: A Tool to Measure Single Molecules," Ph.D dissertation (University of Basel, 2005).

[17]A. I. Yanson, G. Rubio Bollinger, H. E. van den Brom, N. Agraït, and J. M. van Ruitenbeek, Nature **395**, 783 (1998).

[18]S. Bahn and K. W. Jacobsen, Phys. Rev. Lett. **87**, 266101 (2001).

[19]C. Untiedt, A. I. Yanson, R. Grande, G. Rubio-Bollinger, N. Agraït, S. Vieira, and J. M. van Ruitenbeek, Phys. Rev. B. **66**, 085418 (2002).

[20]K. H. Gundlach, Solid-State Electron. **9**, 949 (1966).

[21]Yu. Kolesnychenko, O. I. Shklyarevskii, and H. van Kempen Rev. Sci. Instrum. **70**, 1442 (1999).

[22]H. B. Michaelson, J. Appl. Phys. **48**, 4729 (1977).

[23]J. G. Simmons, J. Appl. Phys. **34**, 1793 (1963).

[24]G. Binnig, N. Garcia, H. Rohrer, J. M. Soler, and F. Flores, Phys. Rev. B. **30**, 4816 (1984).

[25]R. J. P. Keijsers, O. Voets, O. I. Shklyarevskii, and H. van Kempen, Low Temp. Phys. **24**, 730 (1998).

[26]L. Olesen, M. Brandbyge, M. R. Sørensen, K. W. Jacobsen, E. Lægsgaard, I. Stensgaard, and F. Besenbacher, Phys. Rev. Lett. **76**, 1485 (1996).

[27]C. Untiedt, M. J. Caturla, M. R. Calvo, J. J. Palacios, R. C. Segers, and J. M. van Ruitenbeek, Phys. Rev. Lett. **98**, 206801 (2007).

[28]I. K. Yanson, O. I. Shklyarevskii, S. Csonka, H. van Kempen, S. Speller, A. I. Yanson, and J. M. van Ruitenbeek, Phys. Rev. Lett. **95**, 256806 (2005).